On the interplay of waveguide modes and leaky modes in corrugated OLEDs

Julian Hauss,[1,2,*] Tobias Bocksrocker,[1] Boris Riedel,[1,2] Uli Lemmer,[1] and Martina Gerken[2]

[1]*Light Technology Institute, Karlsruhe Institute of Technology (KIT), Kaiserstr. 12, D-76131 Karlsruhe, Germany*
[2]*Institute of Electrical and Information Engineering, Christian-Albrechts-Universität zu Kiel, Kaiserstr. 2, D-24143 Kiel, Germany*
**julian.hauss@kit.edu*

Abstract: Bragg gratings incorporated into organic light-emitting diodes (OLEDs) establish a coupling between waveguide modes and useful light (leaky modes). Here we demonstrate that the net coupling direction depends on the OLED stack design. We fabricated two different device structures with gold Bragg gratings. Angle resolved electroluminescence spectra were recorded. For the first device peaks of enhanced emission due to the Bragg grating are observed corresponding to a net energy transfer in direction of the leaky modes. The second device, on the other hand, exhibits dips in the emission spectrum. This reversed direction of energy transfer from the leaky modes to the waveguide modes is explained considering transfer matrix simulations of modal intensity distributions and device emission simulations. An OLED efficiency enhancement is only achieved, if the waveguide mode extraction is dominant.

OCIS codes: (230.3670) Light-emitting diodes; (250.3680) Light-emitting polymers; (230.7390) Waveguides, planar; (050.1950) Diffraction gratings; (050.2770) Gratings.

References and links

1. C. W. Tang, and S. A. VanSlyke, "Organic electroluminescent diodes," Appl. Phys. Lett. **51**(12), 913 (1987).
2. R. Friend, R. Gymer, A. Holmes, J. Burroughes, R. Marks, C. Taliani, D. Bradley, D. A. Dos Santos, J. Bredas, M. Lögdlun, and W. R. Salaneck, "Electroluminescence in conjugated polymers," Nature **397**(6715), 121–128 (1999).
3. S. Reineke, F. Lindner, G. Schwartz, N. Seidler, K. Walzer, B. Lüssem, and K. Leo, "White organic light-emitting diodes with fluorescent tube efficiency," Nature **459**(7244), 234–238 (2009).
4. S. R. Forrest, "The path to ubiquitous and low-cost organic electronic appliances on plastic," Nature **428**(6986), 911–918 (2004).
5. C. Adachi, M. Baldo, M. E. Thompson, and S. R. Forrest, "Nearly 100% internal phosphorescence efficiency in an organic light-emitting device," J. Appl. Phys. **90**(10), 5048 (2001).
6. S. R. Forrest, M. A. Baldo, D. F. O'Brien, Y. You, A. Shoustikov, S. Sibley, and M. E. Thompson, "Highly efficient phosphorescent emission from organic electroluminescent devices," Nature **395**(6698), 151–154 (1998).
7. N. C. Greenham, R. H. Friend, and D. D. C. Bradley, "Angular dependence of the emission from a conjugated polymer light-emitting diode: implications for efficiency calculations," Adv. Mater. **6**(6), 491–494 (1994).
8. M.-H. Lu, and J. C. Sturm, "Optimization of external coupling and light emission in organic light-emitting devices: modeling and experiment," J. Appl. Phys. **91**(2), 595 (2002).
9. N. K. Patel, S. Cina, and J. H. Burroughes, "High-efficiency organic light-emitting diodes," IEEE J. Sel. Top. Quantum Electron. **8**(2), 346–361 (2002).
10. A. Chutinan, K. Ishihara, T. Asano, M. Fujita, and S. Noda, "Theoretical analysis on light-extraction efficiency of organic light-emitting diodes using FDTD and mode-expansion methods," Org. Electron. **6**(1), 3–9 (2005).
11. W. L. Barnes, "Electromagnetic crystals for surface plasmon polaritons and the extraction of light from emissive devices," J. Lightwave Technol. **17**(11), 2170–2182 (1999).
12. G. Gu, D. Z. Garbuzov, P. E. Burrows, S. Venkatesh, S. R. Forrest, and M. E. Thompson, "High-external-quantum-efficiency organic light-emitting devices," Opt. Lett. **22**(6), 396–398 (1997).
13. S. Nowy, B. C. Krummacher, J. Frischeisen, N. A. Reinke, and W. Brütting, "Light extraction and optical loss mechanisms in organic light-emitting diodes: Influence of the emitter quantum efficiency," J. Appl. Phys. **104**(12), 123109 (2008).
14. H. Greiner, "Light Extraction from Organic Light Emitting Diode Substrates: Simulation and Experiment," Jpn. J. Appl. Phys. **46**(No. 7A), 4125–4137 (2007).

#144577 - $15.00 USD Received 21 Mar 2011; revised 1 Jun 2011; accepted 3 Jun 2011; published 20 Jun 2011

15. B. Riedel, J. Hauss, U. Geyer, J. Guetlein, U. Lemmer, and M. Gerken, "Enhancing outcoupling efficiency of indium-tin-oxide-free organic light-emitting diodes via nanostructured high index layers," Appl. Phys. Lett. **96**(24), 243302 (2010).
16. B. Riedel, I. Kaiser, J. Hauss, U. Lemmer, and M. Gerken, "Improving the outcoupling efficiency of indium-tin-oxide-free organic light-emitting diodes via rough internal interfaces," Opt. Express **18**(Suppl 4), A631–A639 (2010).
17. M. Fujita, K. Ishihara, T. Ueno, T. Asano, S. Noda, H. Ohata, T. Tsuji, H. Nakada, and N. Shimoji, "Optical and electrical characteristics of organic light-emitting diodes with two-dimensional photonic crystals in organic/electrode layers," Jpn. J. Appl. Phys. **44**(No. 6A), 3669–3677 (2005).
18. J. M. Lupton, B. J. Matterson, I. D. W. Samuel, M. J. Jory, and W. L. Barnes, "Bragg scattering from periodically microstructured light emitting diodes," Appl. Phys. Lett. **77**(21), 3340 (2000).
19. U. Geyer, J. Hauss, B. Riedel, S. Gleiss, U. Lemmer, and M. Gerken, "Large-scale patterning of indium tin oxide electrodes for guided mode extraction from organic light-emitting diodes," J. Appl. Phys. **104**(9), 093111 (2008).
20. T.-W. Koh, J.-M. Choi, S. Lee, and S. Yoo, "Optical outcoupling enhancement in organic light-emitting diodes: highly conductive polymer as a low-index layer on microstructured ITO electrodes," Adv. Mater. **22**(16), 1849–1853 (2010).
21. Y. Sun, and S. R. Forrest, "Enhanced light out-coupling of organic light-emitting devices using embedded low-index grids," Nat. Photonics **2**(8), 483–487 (2008).
22. J. Hauss, B. Riedel, S. Gleiss, U. Geyer, U. Lemmer, and M. Gerken, "Periodic nanostructuring for guided mode extraction in organic light-emitting diodes," J. Photon. Energy **1**, 011012 (2011).
23. A. G. Fluxim, SETFOS: Semiconducting emissive thin film optics simulator software, http://www.fluxim.com.
24. A. Gombert, B. Bläsi, C. Bühler, P. Nitz, J. Mick, W. Hoßfeld, and M. Niggemann, "Some application cases and related manufacturing techniques for optically functional microstructures on large areas," Opt. Eng. **43**(11), 2525–2533 (2004).
25. V. Bulović, V. Khalfin, G. Gu, P. Burrows, D. Garbuzov, and S. Forrest, "Weak microcavity effects in organic light-emitting devices," Phys. Rev. B **58**(7), 3730–3740 (1998).

1. Introduction

In the last two decades, organic light-emitting diodes (OLEDs) were the subject of intensive studies [1–3]. Nowadays, OLEDs are found in commercial displays and lighting applications with passive and active matrix displays of mobile phones being the dominant application. OLEDs exhibit major benefits such as high power efficiency, Lambertian emission, and a wide color space, tunable by chemical synthesis of appropriate emitter molecules [3,4]. Using phosphorescent emitters, the internal quantum efficiency of OLEDs is reported to reach nearly 100% [5,6]. However, the external quantum efficiency of OLEDs still suffers from a poor light extraction [7–10]. Only about 20% of the generated light leaves the device as useful light (leaky modes), if no further extraction techniques are applied [11–13]. About 50% is trapped in waveguide modes in anode and organic layers and surface plasmon polaritons (SPPs) at the cathode/organic interface. Another 30% of the light is reflected at the substrate/air interface due to total internal reflection. The extraction of these so called substrate modes has been widely studied and is typically achieved by a modification of the glass/air interface [14] or the substrate before processing the OLED [15,16]. The extraction of the waveguide modes in the anode and organic layers is much harder to achieve. Extraction elements must be inside or close to the OLED thin film stack and have to be processable on large-scales to be suitable for commercial applications. In this context, waveguide mode extraction by Bragg scattering at grating structures [11,17–19] (in the following referred to as Bragg gratings) and scattering at micro structures [20,21] has been extensively studied. Following the Bragg grating approach, one usually expects that the introduction of these elements leads to an extraction of the guided modes. In the following we show that this is not necessarily the case and that the extraction efficiency may even be reduced by the grating structure due to incoupling of leaky modes to waveguide modes. In Ref [14]. an analogous effect is discussed for substrate mode extraction structures. Here we present two different polymer OLED designs with shallow one-dimensional gold gratings on top of the ITO layer as well as a reference device without a grating (see Fig. 1). The design of device 1 allows for efficient energy transfer from the fundamental TE waveguide mode to leaky modes. By varying the gold grating thickness and the Super Yellow emitter layer thickness, we realized a second device design, which exhibits energy transfer from leaky modes to the fundamental TE waveguide mode and thus a reduced overall efficiency. We fabricated and experimentally characterized the devices. Furthermore, we performed transfer matrix (T-matrix) calculations of the waveguide modes in the OLEDs

#144577 - $15.00 USD Received 21 Mar 2011; revised 1 Jun 2011; accepted 3 Jun 2011; published 20 Jun 2011

[22] and the emitter coupling to leaky modes with the software *Setfos* from *Fluxim AG* [23]. The comparison of simulation and experimental results allows for identification of the processes and parameters important for efficient waveguide mode extraction.

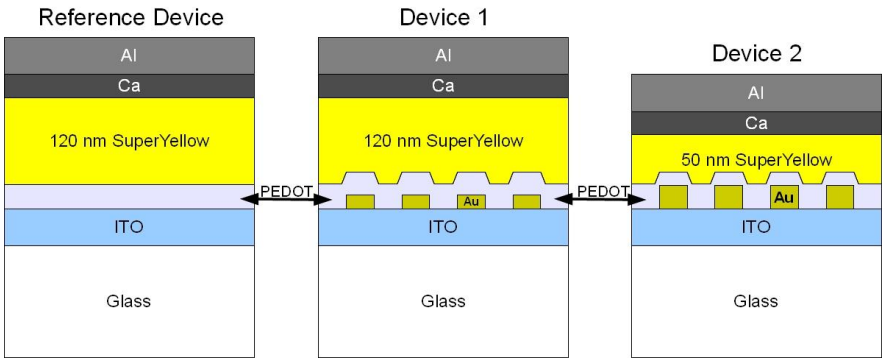

Fig. 1. Schematic of the reference device and two different devices with anode side gold gratings (dimensions not to scale).

2. Grating and device fabrication

2.1 Grating fabrication

One-dimensional gold Bragg gratings were fabricated by laser interference lithography (LIL). LIL allows for a rapid processing of nano-scale grating structures on large areas up to the square meter range [24]. We used standard prefabricated glass substrates with a 130 nm thick ITO layer as starting point. They were coated with photoresist and subsequently exposed to a periodic light pattern formed by the superposition of two expanded beams of an Ar^+ laser with a wavelength of 363.8 nm. The angle of the two beams determines the period of the interference pattern and thus the grating period, which was chosen to be Λ = 375 nm. After development of the resist, a gold-layer was evaporated under high vacuum onto the samples. By using a lift-off process the gold grating was obtained. For device 1 the grating depth was 15 nm; for device 2 the grating depth was 30 nm. The lift-off process was performed in two steps. Firstly, the samples were immersed into acetone for one hour, and subsequently treated in an ultrasonic bath for 15-30 s to remove the remaining photoresist.

2.2 OLED fabrication

The reference device was fabricated directly on top of an ITO-covered glass substrate without a gold grating. To fabricate device 1 and device 2, polymer OLEDs were fabricated on top of ITO-covered glass substrates with gold gratings. To this end, the substrates covered with ITO and gold gratings were cleaned with isopropyl and acetone in an ultrasonic bath and subsequently exposed to oxygen plasma to increase the ITO-workfunction and to remove the organic residues. The following steps were performed in a glovebox with nitrogen atmosphere. As a hole-transport layer a PEDOT:PSS (Clevios PH 500 purchased from H.C. Starck, diluted with H_2O at a ratio 1:1) was spincoated at a speed of 2000 rpm, resulting in a 30 nm thick layer. As a polymeric emitter the phenylene substituted poly(para-phenylenevinylene) (Ph-PPV; "SuperYellow" purchased from Merck OLED Materials GmbH) was spincoated at 1000 rpm. We used SuperYellow dissolved in toluene and fabricated device 1 and the reference device with a 120 nm SuperYellow layer and device 2 with a layer thickness of 50 nm. Finally, a cathode consisting of a 50 nm layer of calcium and a 200 nm layer of aluminum was evaporated at a pressure of 10^{-7} mbar. Since the characterization of the devices was carried out under ambient conditions, the OLEDs were encapsulated using an epoxy resin adhesive and a glass cover.

#144577 - $15.00 USD Received 21 Mar 2011; revised 1 Jun 2011; accepted 3 Jun 2011; published 20 Jun 2011

3. Measurement and experimental results

To investigate the effect of the gratings on the interplay of waveguide modes and leaky modes we performed angle resolved electroluminescence spectra measurements. The measurements were carried out at room temperature using a source-measure unit (Keithley SMU 236), a spectrometer (Acton Research Corporation SpectraPro-300i) with an intensified charge-coupled device (ICCD) (Princeton Instruments PiMax:512) and a multimode fiber. The OLEDs emission spectra were recorded in a plane perpendicular to the grating grooves of the one-dimensional gold grating. A scheme of the setup is given in Fig. 2.

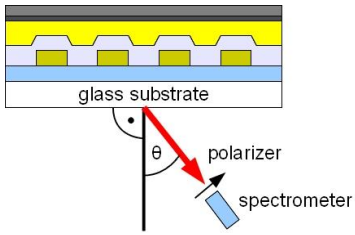

Fig. 2. Schematic of the measurement setup used for angle resolved electroluminescence emission measurements. For the devices 1 and 2 the spectra were recorded in a plane perpendicular to the grating grooves.

Figures 3(a)-3(c) show the angle resolved emission of the reference OLED without gold grating, device 1 and device 2. It is clearly visible that the overall angular and spectral emission of the two gold grating devices is different from the emission of the reference device. The introduction of the gold grating modifies the microcavity of the OLEDs and thus the coupling of the leaky modes to the emitter. For device 1 this leads to a spectral red shift in the emission whereas the emission of device 2 is blue shifted.

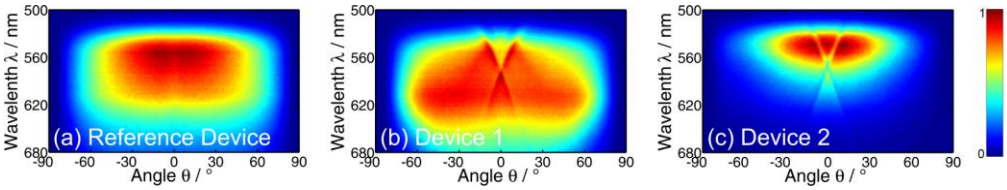

Fig. 3. Angle resolved electroluminescence emission spectra of (a) the reference device, (b) device 1, and (c) device 2.

Measurements in an Ulbricht sphere yielded that device 1 exhibits about 25% enhanced power efficiency compared to the reference device, whereas device 2 only reaches 70-75% of the power efficiency of the reference device. These changes in efficiency are mainly attributed to waveguide mode extraction and different environments (cavities) of the emitters. A more detailed analysis of the latter will be given elsewhere. Here, we want to focus on Bragg scattering effects of the grating on the waveguide mode. In Fig. 3(b) the emission of device 1 exhibits peaks at certain angles $\theta(\lambda)$ whereas the emission of device 2 exhibits dips at similar angles (Fig. 3(c)). The emission of the reference device shows neither peaks nor dips. Figures 4(a) and 4(b) show the emission of device 1 and device 2 as a function of the emission angle to air at the SuperYellow peak emission wavelength of $\lambda = 550$ nm. In Fig. 4(c) the polarized emission of device 1 is given, indicating that the peaks are associated to TE-polarized emission.

#144577 - $15.00 USD Received 21 Mar 2011; revised 1 Jun 2011; accepted 3 Jun 2011; published 20 Jun 2011

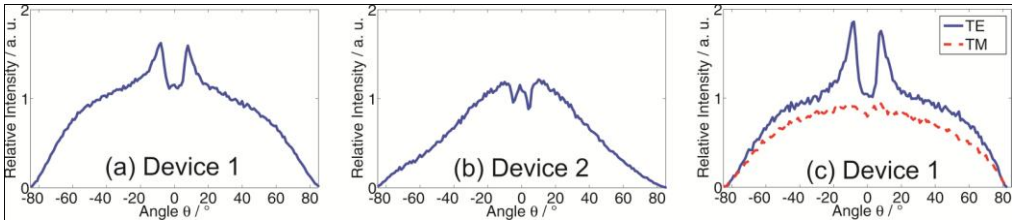

Fig. 4. Electroluminescence emission of (a) device 1, (b) device 2 at a wavelength of 550 nm. (c) Emission of device 1 separated into TE- and TM-polarization.

4 Discussion and simulation

In order to explain why the emission of device 1 exhibits peaks whereas the emission of device 2 exhibits dips, we discuss the coupling of waveguide modes to leaky modes in more detail. Optical modes can be classified by the in-plane wave vector k_x. Figure 5 shows a general classifications of optical modes in OLEDs in a dispersion diagram $\omega(k_x)$. The leaky mode region of light that is able to leave the device is located above the so called air light line. Below the air light line and above the glass light line the substrate mode continuum is found. Below the glass light line, we find discrete waveguide modes.

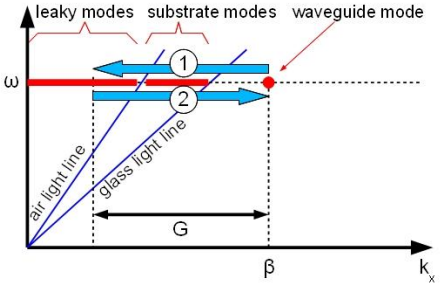

Fig. 5. Classification of optical modes in OLEDs in a dispersion diagram $\omega(k_x)$. The leaky mode continuum of the light that is able to leave the device is located above the air light line. The substrate mode continuum is located between the air light line and the glass light line. Discrete waveguide modes are found below the glass light line. Arrow 1 represents the extraction of a waveguide mode to the leaky modes by Bragg scattering at a grating with reciprocal lattice constant *G*. Arrow 2 represents the inverse process: Light from the leaky mode region being coupled into the waveguide mode by a Bragg grating with reciprocal lattice constant *G*.

The introduction of a Bragg grating couples modes with different in-plane wave vectors by Bragg scattering $k_x' = k_x \pm m \cdot G$. Here, k_x' and k_x are the in-plane wave vector components perpendicular to the grating grooves after and before the scattering event. $G = 2\pi/\Lambda$ is the reciprocal lattice constant of the grating with a grating period Λ. The integer value m specifies the scattering order. In the following, we focus on the first order with $m = 1$.

The extraction of a waveguide mode characterized by its propagation constant β to a leaky mode k_x' above the light line is then described by the equation

$$k_x' = \beta - G. \tag{1}$$

This process is represented in Fig. 5 by arrow 1 and the associated extraction angle to air is

$$\theta(\Lambda, \lambda_0) = \arcsin(n_{eff} - \lambda_0 / \Lambda), \tag{2}$$

with the effective index of refraction $n_{eff} = \beta / \left|\vec{k}_0\right|$ of the waveguide mode.

#144577 - $15.00 USD Received 21 Mar 2011; revised 1 Jun 2011; accepted 3 Jun 2011; published 20 Jun 2011

For both gold grating devices, we performed one-dimensional transfer matrix calculations of the waveguide modes in the OLED thin film structure, treating the gold grating layer like a homogeneous effective material with averaged optical properties of air and gold. The calculated propagation constants of the fundamental TE mode together with Eq. (2) were used to calculate the mode extraction angles θ for device 1. A comparison of the calculated angles (solid line) and the measured extraction angles (dots) is given in Fig. 6(a) and associates the extraction peaks with first order Bragg scattering of the fundamental TE mode. The modal electric field intensity at a wavelength of 550 nm is given in Fig. 6(b).

In device 2 the situation is different. The dips for device 2 with the 50 nm SuperYellow layer can be explained by the inverse process to Eq. (1):

$$\beta = k_x' = k_x + G, \tag{3}$$

which describes the incoupling of light from leaky modes k_x into the waveguide mode β by Bragg scattering. In Fig. 5, this process is represented by arrow 2. T-matrix calculations of the fundamental TE mode of device 2 together with Eq. (3) were used to calculate the dip positions θ(λ). A comparison of the calculations with the measured dip positions is given in Fig. 6(c). Figure 6(d) shows the fundamental TE mode electric field intensity in device 2.

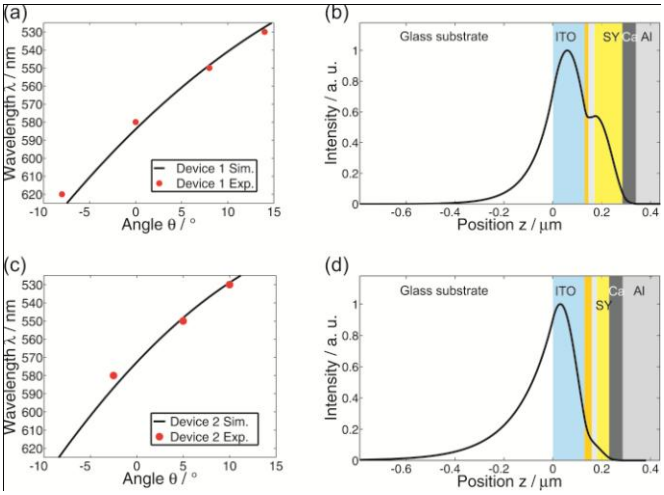

Fig. 6. (a) Comparison of experimental and calculated spectral and angular position of the fundamental TE waveguide mode in device 1. (b) T-Matrix simulation of the normalized electric field intensity of the fundamental TE mode in device 1 at a wavelength of 550 nm. (c) Comparison of experimental and calculated spectral and angular position of the fundamental TE waveguide mode in device 2. (d) T-matrix simulation of the normalized electric field intensity of the fundamental TE mode in device 2 at a wavelength of 550 nm.

Typically, in OLEDs coupling takes place in both directions – from waveguide modes to leaky modes and vice versa. In the following we want to address the question why in device 1 the first process according to Eq. (1) is dominant and in device 2 the second process described by Eq. (3) dominates. Starting from Fermi's golden rule the transition probability of an excited exciton in an OLED into a TE mode can be written as [25]:

$$W^{TE} = W_0 \frac{\pi}{2 n_{org} k_0} \frac{\left|E_{\parallel}(z_e)\right|^2}{\int \left|E_{\parallel}(z)\right|^2 dz}, \tag{4}$$

with the intrinsic radiative transition rate W_0, the refractive index of the emitter material n_{org} and the wavevector in vacuum k_0. $E_{\parallel}$ is the in plane electric field component of a certain mode, z the direction normal to the OLED surface and z_e the emitter zone position in the device. Thus, the last fraction in Eq. (4) is a measure for the electric field intensity of a certain

#144577 - $15.00 USD Received 21 Mar 2011; revised 1 Jun 2011; accepted 3 Jun 2011; published 20 Jun 2011

mode at the emitter position. Figure 6(b) and 6(d) show the fundamental TE mode intensity distribution of device 1 and device 2 at a wavelength of 550 nm. The electrical field intensity of the TE waveguide mode in the emission layer of device 1 is much higher than in device 2. This indicates that in device 1 the waveguide modes are stronger populated compared to device 2. In order to investigate the coupling of the emitter to waveguide modes and leaky modes in more detail we made use of the software *Setfos* from *Fluxim AG* [23]. We carried out one-dimensional optical simulation of an emitting dipole in the two different OLED structures. The gold grating was treated as a homogeneous effective material with averaged optical properties of air and gold. We chose the emitters in both devices to have the same intrinsic emission intensity and placed them in the middle of the SuperYellow layer. Figure 7(a) shows the calculated dipole emission as a function of the effective index of refraction n_{eff}. Device 1 exhibits a distinct peak around $n_{eff} = 1.6$ related to the fundamental TE waveguide mode whereas the coupling to leaky modes ($n_{eff} < 1$) is rather weak. For device 2 the situation is opposite. The emission to leaky modes is stronger, but the peak related to the waveguide mode is rather weak. The emitter emits to the leaky mode and the waveguide mode. In addition, the grating couples the waveguide and the corresponding leaky mode. It should be noted that the grating only couples these states; it does not determine the energy transfer direction. The latter is determined by the ratio of the population of the leaky mode and the waveguide mode by the emitter. Furthermore, the waveguide modes are damped, a fact which is mainly attributed to the conductive electrodes having high values of the imaginary part of the index of refraction. This hinders the outcoupling to be more efficient, even if outcoupling dominates over incoupling. On the other hand, leaky modes leave the device and propagate to the far field. This principle is illustrated in Fig. 7(b).

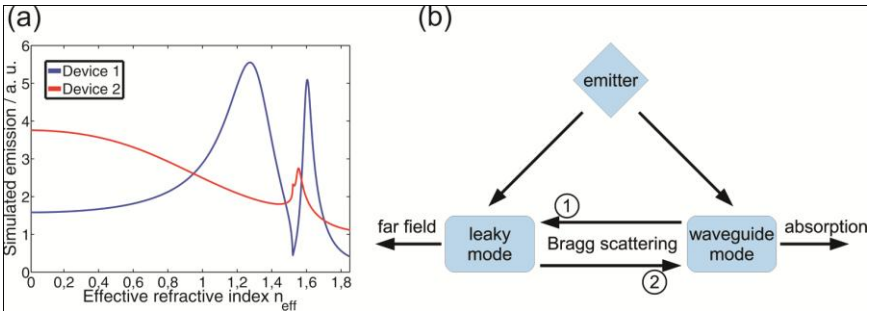

Fig. 7. (a) Simulated dipole emission as a function of the effective index of refraction n_{eff} at a wavelength of 550 nm. Device 1 exhibits a distinct peak around $n_{eff} = 1.6$ related to the fundamental TE waveguide mode, whereas the coupling to leaky modes ($n_{eff} < 1$) is rather weak. For device 2 the situation is opposite. (b) Scheme of the emitter coupling to leaky modes and waveguide modes including grating coupling via Bragg scattering between modes into both directions. Arrow 1 represents the waveguide mode extraction process described by Eq. (1). Arrow 2 represents the incoupling in waveguide modes described by Eq. (3). In addition the waveguide modes are damped due to the conductive electrodes and leaky modes leave the device towards the far field.

The simulations agree well with our experimental findings. For device 1, the light extraction process dominates. In device 2 the process of coupling light from the leaky mode region into the waveguide mode dominates over the light extraction process from the waveguide mode to leaky modes. Neglecting the incoupling process, one could have expected waveguide mode outcoupling peaks also for device 2, even though, the waveguide mode in device 2 is only weakly populated by the emitter. This is of particular importance for more complex OLED structures with several organic layers and more than one waveguide mode. In this case one should avoid that a structure designed to extract a certain mode might lead to unfavorable incoupling into other waveguide modes or SPPs. The important parameters are the emitter coupling to the waveguide mode and to the corresponding leaky mode, to which the waveguide mode is coupled to by the grating. A general guideline or design rule is hard to give as OLED stack design is an optimization task with many parameters. Electrical and

#144577 - $15.00 USD Received 21 Mar 2011; revised 1 Jun 2011; accepted 3 Jun 2011; published 20 Jun 2011

optical requirements have to be fulfilled simultaneously. Nevertheless, our investigation shows that the interplay of in- and outcoupling needs to be considered, when a stack design is developed for OLEDs with waveguide mode extraction elements.

5 Conclusion

We investigated the interplay between waveguide modes and leaky modes considering two different polymer OLEDs with gold gratings. The experimental findings were compared to simulations of the waveguide modes and optical device emission, which allows for explaining the experimental findings. We showed that the stack design and layer thicknesses of the OLEDs have a strong impact on the extraction efficiency. This can even lead to a situation, in which incoupling into waveguide modes dominates over the intended extraction effect. Especially for complex multi-layer OLED designs with several waveguide modes, our findings are of importance for the design of efficient mode extraction structures and the maximization of the overall efficiency of the devices.

Acknowledgments

We acknowledge support by the Bundesministerium für Bildung und Forschung (BMBF) within the project “NanoFutur” (03X5514) and the Karlsruhe School of Optics & Photonics (KSOP).

#144577 - $15.00 USD Received 21 Mar 2011; revised 1 Jun 2011; accepted 3 Jun 2011; published 20 Jun 2011